AMERICAN SOCIETY FOR MICROBIOLOGY | mBio®

RESEARCH ARTICLE
Host-Microbe Biology

Direct Intracellular Visualization of Ebola Virus-Receptor Interaction by *In Situ* Proximity Ligation

Eva Mittler,[a] Tanwee Alkutkar,[a]* Rohit K. Jangra,[a] Kartik Chandran[a]

[a]Albert Einstein College of Medicine, Department of Microbiology & Immunology, Bronx, New York, USA

ABSTRACT Ebola virus (EBOV) entry into host cells comprises stepwise and extensive interactions of the sole viral surface glycoprotein (GP) with multiple host factors. During the intricate process, following virus uptake and trafficking to late endosomal/lysosomal compartments, GP is proteolytically processed to cleaved GP (GP_{CL}) by the endosomal proteases cathepsin B and L, unmasking GP's receptor-binding site. Engagement of GP_{CL} with the universal filoviral intracellular receptor Niemann-Pick C1 (NPC1) eventually culminates in fusion between viral and cellular membranes, cytoplasmic escape of the viral nucleocapsid, and subsequent infection. Mechanistic delineation of the indispensable GP_{CL}-NPC1-binding step has been severely hampered by the unavailability of a robust cell-based assay assessing interaction of GP_{CL} with full-length endosomal NPC1. Here, we describe a novel *in situ* assay to monitor GP_{CL}-NPC1 engagement in intact, infected cells. Visualization of the subcellular localization of binding complexes is based on the principle of DNA-assisted, antibody-mediated proximity ligation. Virus-receptor binding monitored by proximity ligation was contingent on GP's proteolytic cleavage and was sensitive to perturbations in the GP_{CL}-NPC1 interface. Our assay also specifically decoupled detection of virus-receptor binding from steps post-receptor binding, such as membrane fusion and infection. Testing of multiple FDA-approved small-molecule inhibitors revealed that drug treatments inhibited virus entry and GP_{CL}-NPC1 recognition by distinctive mechanisms. Together, here we present a newly established proximity ligation assay, which will allow us to dissect cellular and viral requirements for filovirus-receptor binding and to delineate the mechanisms of action of inhibitors on filovirus entry in a cell-based system.

IMPORTANCE Ebola virus causes episodic but increasingly frequent outbreaks of severe disease in Middle Africa, as shown by the recently overcome second largest outbreak on record in the Democratic Republic of Congo. Despite considerable effort, FDA-approved anti-filoviral therapeutics or targeted interventions are not available yet. Virus host-cell invasion represents an attractive target for antivirals; however, our understanding of the inhibitory mechanisms of novel therapeutics is often hampered by fragmented knowledge of the filovirus-host molecular interactions required for viral infection. To help close this critical knowledge gap, here, we report an *in situ* assay to monitor binding of the EBOV glycoprotein to its receptor NPC1 in intact, infected cells. We demonstrate that our *in situ* assay based on proximity ligation represents a powerful tool to delineate receptor-viral glycoprotein interactions. Similar assays can be utilized to examine receptor interactions of diverse viral surface proteins whose studies have been hampered until now by the lack of robust *in situ* assays.

KEYWORDS NPC1, Ebola virus, glycoprotein, inhibitors, proximity ligation, virus entry

Members of the family *Filoviridae*, including Ebola virus (EBOV), are emerging zoonotic pathogens that cause episodic but increasingly frequent outbreaks of a highly lethal disease in Middle Africa (1). The two largest outbreaks of EBOV disease on record, from 2014 to 2016 in Liberia, Guinea, and Sierra Leone and from 2018 to 2020

Citation Mittler E, Alkutkar T, Jangra RK, Chandran K. 2021. Direct intracellular visualization of Ebola virus-receptor interaction by *in situ* proximity ligation. mBio 12:e03100-20. https://doi.org/10.1128/mBio.03100-20.

Editor Carolyn B. Coyne, University of Pittsburgh School of Medicine

Address correspondence to Kartik Chandran, kartik.chandran@einsteinmed.org.

* Present address: Tanwee Alkutkar, Department of Integrative Structural and Computational Biology, The Scripps Research Institute, La Jolla, California, USA.

Received 11 November 2020
Accepted 16 November 2020
Published 12 January 2021

in the Democratic Republic of Congo, which both included spillover cases to neighboring countries, highlight the potential of filoviruses to cause health emergencies of international scope (51). There is an urgent need for effective countermeasures; however, their development is hindered by our limited understanding of filovirus-host molecular interactions required for viral entry and infection.

The single filovirus-encoded spike glycoprotein (GP) is necessary and sufficient to mediate all steps in viral entry into host cells, culminating in cytoplasmic escape of the viral nucleocapsid. Following endocytosis, virions traffic to late endosomes/lysosomes (LE/LY) (2–5), where GP gains access to multiple essential host factors. GP is proteolytically processed by endosomal cysteine cathepsins B and L (CatB and CatL, respectively), which remove the heavily glycosylated C-terminal glycan cap and mucin domain sequences in the GP_1 subunit (6–8), thereby exposing a recessed receptor-binding site (RBS). This cleaved GP species (GP_{CL}) binds domain C of Niemann-Pick C1 (NPC1), a ubiquitously expressed cholesterol transporter embedded in endo-/lysosomal membranes that acts as a universal intracellular receptor for all filoviruses (9–13). Although GP_{CL}-NPC1 recognition is a prerequisite for downstream steps in virus entry and infection, *in vitro* work suggests that NPC1 binding is not sufficient to trigger large-scale conformational changes in GP or to initiate a subsequent merger of viral and host membranes (14, 15). Indeed, NPC1's precise role beyond GP binding, which presumably provides a physical link between virus particles and host membranes, remains elusive to date.

Because a robust cell-based assay assessing the interaction of GP_{CL} with full-length endosomal NPC1 in its native context has been unavailable, mechanistic studies of this indispensable virus-receptor interaction have been largely limited to *in vitro* assays. These assays are predominantly based on a truncated, soluble form of a single domain in NPC1, domain C, as well as on *in vitro*-cleaved GPs (10, 11). However, studies with NPC1-targeting inhibitors suggest that these assays do not fully recapitulate the authentic interaction(s) between *in situ*-cleaved GP and full-length NPC1 in its membrane context within late endosomes and/or lysosomes (10, 15). To address this gap, we describe herein an *in situ* assay to monitor GP_{CL}-NPC1 binding in individual endosomal compartments of intact, infected cells by using DNA-guided, antibody-mediated proximity ligation. We employed this assay to show that GP_{CL}-NPC1 interaction is restricted to the lumina of NPC1-positive ($NPC1^+$) LE/LY, is contingent on the proteolytic cleavage of GP, and is sensitive to the mutational disruption of the GP_{CL}-NPC1 interface. Testing of multiple FDA-approved small-molecule inhibitors in our assay revealed that drug treatments inhibited virus entry and GP_{CL}-NPC1 recognition by distinct mechanisms. Application of this assay will allow us to dissect the cellular and viral requirements for filovirus-receptor interaction and to delineate the mechanisms of action of small-molecule inhibitors on filovirus entry.

RESULTS

Development of an assay visualizing EBOV GP-NPC1 binding in intact cells by *in situ* proximity ligation. During viral entry, proteolytically cleaved forms of EBOV GP (GP_{CL}) interact with their critical endosomal receptor NPC1. We postulated that an *in situ* proximity ligation assay (PLA) could be used to monitor this essential binding step in intact cells. To detect viral particles, we used a recombinant vesicular stomatitis virus (rVSV) containing the viral phosphoprotein P linked to a fluorescent monomeric NeonGreen (mNG-P) protein and bearing EBOV GP (16). Viral particles were allowed to attach at 4°C to U2OS human osteosarcoma cells stably expressing NPC1 tagged with a blue fluorophore, eBFP2 (16), and the cells were then shifted to 37°C to allow synchronized viral internalization. Visualization of fixed $U2OS^{NPC1\text{-}eBFP2}$ cells by fluorescence microscopy revealed that most internalized viral particles reached NPC1-containing late endosomes ($NPC1^+$ LE) within 60 min (Fig. 1).

To detect closely apposed GP_{CL} and NPC1 molecules in infected cells, we incubated them with oligonucleotide-linked monoclonal antibodies directed against each protein; GP's highly conserved receptor-binding site (RBS), unmasked by proteolytic cleavage to GP_{CL} in endosomes, was detected with the RBS-specific antibody MR72 (16–18),

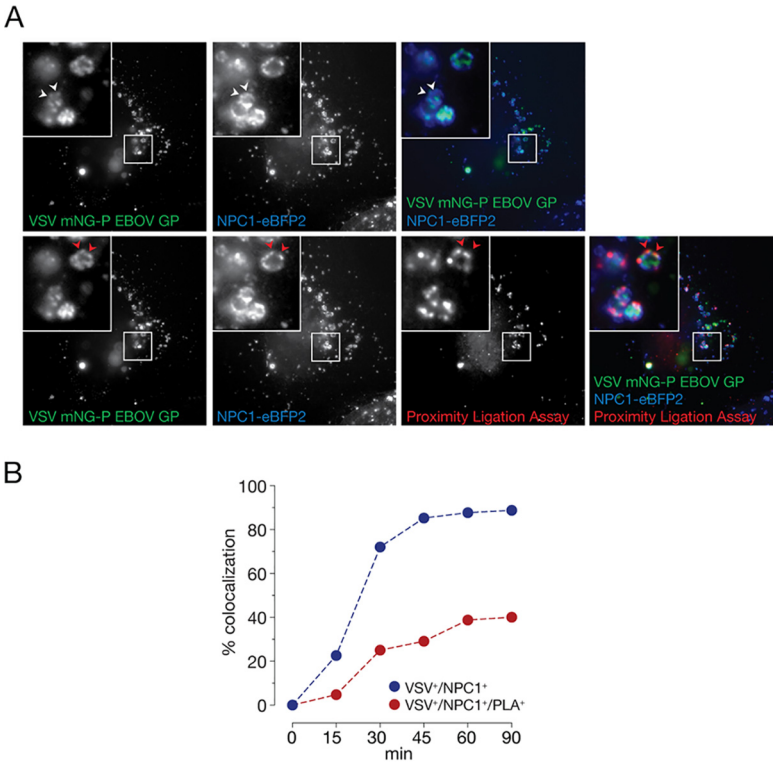

FIG 1 Development of an EBOV GP-NPC1 binding assay in intact cells by *in situ* proximity ligation. (A) VSV mNG-P particles bearing EBOV GP were internalized into U2OS cells ectopically expressing NPC1-eBFP2 for 60 min. Cells were fixed, permeabilized, and subjected to proximity ligation assay (PLA) using GP_{CL}- and NPC1-specific antibodies (MR72/MAb-548). During amplification, resulting PLA products were labeled with a detector oligonucleotide conjugated with a red fluorophore. White arrowheads, VSV/NPC1 colocalization; red arrowheads, VSV/NPC1/PLA colocalization. (B) VSVs bearing EBOV GP were endocytosed into U2OS cells as described in panel A, fixed at the indicated time points, and subjected to PLA. VSV-positive compartments (VSV^+) were enumerated; the percentages of compartments also positive for NPC1 ($VSV^+/NPC1^+$) or NPC1 plus PLA ($VSV^+/NPC1^+/PLA^+$) were determined. Averages of pooled cells out of two independent experiments are shown ($n \geq 30$ per time point).

and NPC1 was detected with the domain C-specific monoclonal antibody MAb-548 (16). Based on the rough size of the oligonucleotide-linked MAbs used, we estimate that the maximum distance between GP_{CL} and NPC1 molecules amounts to approximately 20 nm (19). Circular DNA molecules were generated by oligonucleotide-guided proximity ligation, amplified *in situ*, and visualized with a fluorophore-conjugated detector oligonucleotide (20, 21). The PLA signal required the addition of both MR72 and MAb-548 antibodies and was only observed in cells that were allowed to internalize viral particles (Fig. S1 in the supplemental material). Also, the PLA signal colocalized with VSV mNG-P particles bearing EBOV GP in the lumina of $NPC1^+$ LE (Fig. 1A). Proximity ligation and viral trafficking to $NPC1^+$ LE displayed similar kinetics; both peaked within 60 min post-viral uptake, followed by a plateau phase (Fig. 1A and B). Although most internalized viral particles trafficked to and colocalized with $NPC1^+$ compartments (Fig. 1B), only a subset of these $VSV^+/NPC1^+$ vesicles also displayed a PLA signal (Fig. 1B). Accordingly, in the following studies aimed at determining the viral and cellular requirements for proximity-dependent ligation of GP_{CL}- and NPC1-specific antibodies, we routinely enumerated the number of $VSV^+/NPC1^+$ compartments per cell and reported the percentage of these compartments that were also positive for PLA signal ($VSV^+/NPC1^+/PLA^+$).

Proximity ligation is sensitive to perturbations in the GP_{CL}-NPC1 domain C interface. Specific interactions of EBOV GP with NPC1 domain C have been mapped to amino acid residues in the GP_1 subunit that are exposed upon proteolytic cleavage (10,

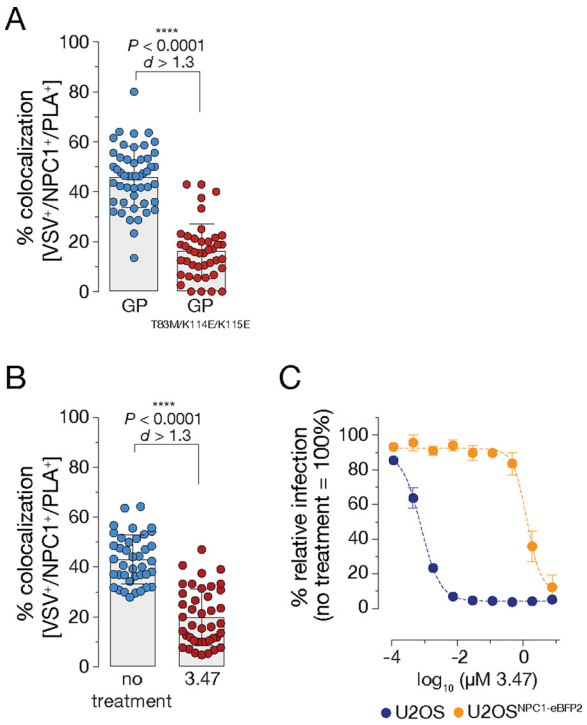

FIG 2 Proximity ligation is sensitive to perturbations in the GP_{CL}-NPC1 domain C interface. (A) VSV mNG-P particles bearing EBOV GP or EBOV $GP^{T83M/K114E/K115E}$ were internalized into $U2OS^{NPC1\text{-}eBFP2}$ cells for 60 min followed by cell fixation, permeabilization, and PLA. Cells were analyzed by fluorescence microscopy; data points represent the percentage of $VSV^+/NPC1^+/PLA^+$ compartments per individual cell; bars depict the pooled averages and standard deviations (± SD) for all cells from two independent experiments ($n \geq 40$). An unpaired two-tailed *t* test was used to compare $VSV^+/NPC1^+/PLA^+$ compartments of cells infected by VSV bearing either EBOV GP or EBOV $GP^{T83M/K114E/K115E}$ (****, $P < 0.0001$). Group means calculated from the percentage of $VSV^+/NPC1^+/PLA^+$ vesicles were compared by Cohen's *d* effect size ($d > 1.3$). (B) $U2OS^{NPC1\text{-}eBFP2}$ cells were preincubated with the inhibitor 3.47 (1 μM) for 60 min at 37°C followed by VSV mNG-P EBOV GP uptake for 60 min and PLA. Data points were acquired and analyzed as described in panel A. (C) After preincubation of $U2OS^{NPC1\text{-}eBFP2}$ and wild-type U2OS cells with increasing 3.47 concentrations, cells were infected with VSV mNG-P EBOV GP for 16 h. Infection was measured by automated counting of mNG^+ cells and normalized to infection obtained in the absence of 3.47. Averages ± SD for six technical replicates pooled from two independent experiments are displayed. Data were subjected to nonlinear regression analysis to derive 3.47 concentration at half-maximal inhibition of infection (IC_{50} ± 95% confidence intervals for nonlinear curve fit).

17, 22). Mutations of the charged surface-exposed amino acids K114 and K115 and the polar amino acid T83 led to significant defects in NPC1 binding and viral entry (4, 17). To determine if these mutations impact proximity ligation, we exposed cells to VSVs bearing $GP^{T83M/K114E/K115E}$. Virions were efficiently trafficked to $NPC1^+$ LE and underwent GP_1 cleavage, as indicated by detection of the GP_1 RBS with the MAb MR72. However, viral infectivity was greatly diminished (Fig. S2A and B). Concordantly, we observed a significant reduction of $VSV^+/NPC1^+/PLA^+$ colocalization, suggesting that GP_{CL}-NPC1 engagement in LE is necessary for PLA signal formation (Fig. 2A).

The small-molecule filovirus entry inhibitor 3.47 was described to block EBOV GP-dependent entry and infection potentially by interfering with GP_{CL}-NPC1 recognition (11). Accordingly, we directly compared the effect of 3.47 on viral entry in wild-type U2OS cells expressing basal levels of NPC1 against that in $U2OS^{NPC1\text{-}eBFP2}$ cells used for the PLA (Fig. 2C). Consistent with its activity as an NPC1-targeting inhibitor, and as shown previously (11), 3.47's antiviral activity was substantially attenuated in cells overexpressing NPC1, but we were nevertheless able to identify a concentration (1 μM) that afforded ~50% inhibition of viral entry; higher concentrations of 3.47 were cytotoxic. Pretreatment of $U2OS^{NPC1\text{-}eBFP2}$ cells with 3.47 at 1 μM significantly reduced, but

did not entirely block PLA signal; we suggest that the observed residual signal is based on that the applied 3.47 concentration is not sufficient to counteract cellular NPC1 entirely (Fig. 2B). However, the small-molecule incubation did not modify NPC1$^+$ LE morphology, block viral trafficking and GP cleavage, or influence detection by the assay antibodies, MR72 and MAb-548 (Fig. S2C). Our data that both genetic and pharmacological disruptions of the virus-receptor interface inhibit PLA strongly suggest that this assay indeed monitors GP_{CL}-NPC1 domain C engagement in endosomal compartments.

Detection of GP_{CL}-NPC1 binding by PLA requires endosomal cleavage of GP. Endosomal host cysteine cathepsins B and L (CatB and CatL, respectively) are key mediators of the entry-related GP→GP_{CL} cleavage that is required for GP_{CL}-NPC1 binding and viral membrane fusion (4, 6–8). Their inactivation by pan-cysteine cathepsin inhibitors, including E-64 and E-64d, blocks filovirus entry (6, 7) (Fig. S3A). Concordantly, we found that pretreatment of cells with E-64d abolished both GP cleavage (and consequently exposure of the GP_1 NPC1-binding site recognized by MR72) (Fig. 3B) and GP_{CL}-NPC1 engagement as measured by PLA (Fig. 3A). Intriguingly, previous work has also hinted at the existence of cellular target(s) of E-64 in addition to CatB and CatL, whose inhibition imposes one or more blocks to viral entry (6, 7, 23, 24). To further investigate the cysteine protease-dependent EBOV entry mechanism, we generated *CatB/L*-knockout (KO) U2OS cell lines by CRISPR/Cas9 genome engineering (Fig. S4A). As expected, the *CatB/L*-KO cells lacked CatB and CatL activity and were substantially resistant to EBOV GP-dependent entry (Fig. S4B and C). Surprisingly, however, and in contrast to our findings in E-64d treated cells, viral particles underwent efficient exposure of the NPC1-binding site (and MR72 epitope) in GP in *CatB/L*-KO cells (Fig. 3B). Despite this apparent capacity for GP cleavage in the absence of CatB and CatL, viral particles were nevertheless unable to engage NPC1 as measured by PLA (Fig. 3A).

GP priming in viral entry can be recapitulated *in vitro* by incubating rVSV bearing full-length EBOV GP with CatL or the bacterial protease thermolysin (THL) which mimics CatL/B cleavage (7); both cleave off GP_1 sequences corresponding to the glycan cap and mucin domain. Increased infectivity of viral particles bearing THL/CatL-cleaved GPs was reported previously and can be attributed to improved cell binding of virions as well as increased accessibility of the GP's RBS for NPC1 domain C interaction (6, 10, 25) (Fig. S3B). *In vitro* cleavage of GP significantly enhanced GP_{CL}-NPC1 domain C binding *in situ* by 1.5- to 2-fold, indicating that proteolytic processing of GP is indispensable for detection of virus-receptor interaction by proximity ligation (Fig. 3C). In order to determine possible requirements for additional cysteine protease activity pre-NPC1 binding, we evaluated proximity ligation with THL-cleaved GP in the presence of the pan-cysteine cathepsin inhibitor E-64d. Here, the absence of cysteine protease proteolytic activity did not affect GP_{CL}-NPC1 engagement (Fig. 3D), suggesting the existence of an E-64d-sensitive downstream entry block post-NPC1 binding, as proposed previously (4, 23).

***In situ* proximity ligation decouples GP_{CL}-NPC1 interaction from post-binding entry steps.** As one of the critical steps in viral entry, GP-NPC1 interaction is the starting point for subsequent post-binding entry processes, including, among others, membrane fusion triggering, cytoplasmic nucleocapsid escape, and infection (4, 9–11). To examine if the established *in situ* PLA selectively monitored GP_{CL}-NPC1 engagement or, in addition, also downstream steps such as membrane fusion, we made use of an EBOV GP mutant harboring amino acid substitutions in the GP_1 internal fusion loop, $GP^{L529A/I544A}$. Amino acids L529 and I544 were shown to form a fusogenic hydrophobic surface at the tip of the fusion loop and proposed to be crucial for insertion of the loop into host membranes and subsequent membrane fusion steps (26, 27). Late-endosomal delivery of VSV bearing $GP^{L529A/I544A}$ and exposure of GP's RBS did not differ substantially from those of VSV harboring wild-type GP. However, steps post NPC1-binding, including membrane fusion triggering and virus infection, were inhibited (4) (Fig. S5A). Consistent with these observations, *in situ* proximity ligation of VSV bearing $GP^{L529A/I544A}$ resembled that obtained with VSV decorated with wild-type GP (Fig. 4A).

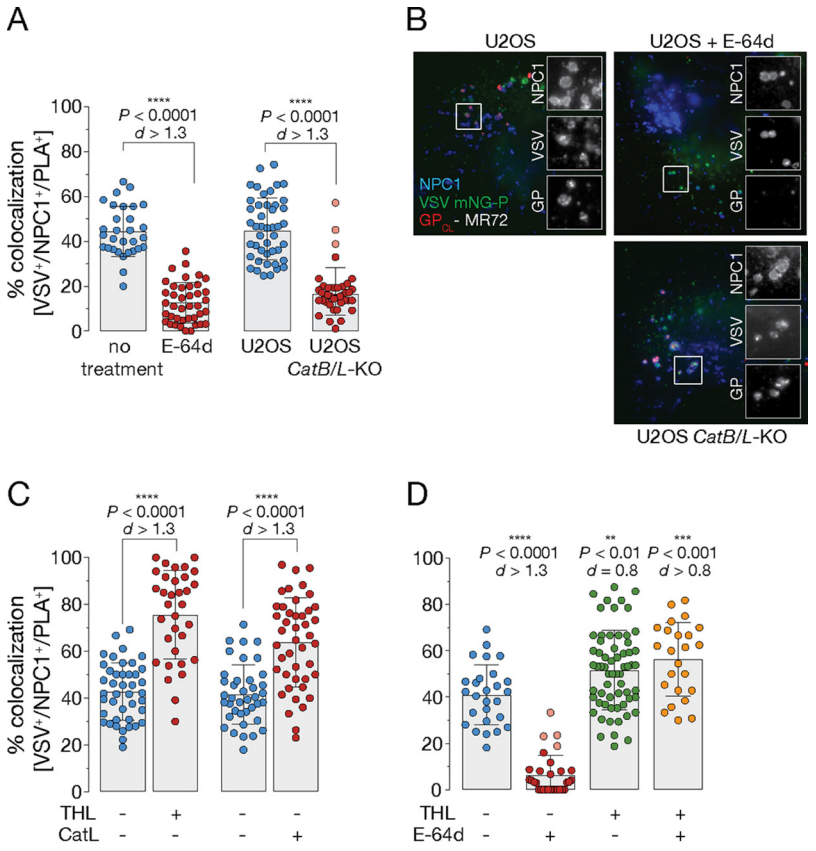

FIG 3 Detection of GP_{CL}-NPC1 binding by PLA requires endosomal cleavage of GP. (A) VSV mNG-P particles bearing EBOV GP were incubated with either $U2OS^{NPC1\text{-}eBFP2}$ cells pretreated with E-64d (100 mM for 6 h at 37°C) (left) or U2OS *CatB/L*-KO cells ectopically overexpressing Flag-tagged NPC1 (right). Cells were fixed following virus incubation (1 h at 37°C), permeabilized, and subjected to PLA. Data points represent the percentage of $VSV^+/NPC1^+/PLA^+$ compartments per individual cell; bars depict the average ± SD for all data points pooled from two independent experiments ($n \geq 30$). Points with reduced transparency represent values outside the 10th to 90th percentiles. An unpaired two-tailed *t* test was used to compare $VSV^+/NPC1^+/PLA^+$ compartments of wild-type cells with either inhibitor-treated (left) or KO (right) cells infected by EBOV GP-decorated VSV (****, $P < 0.0001$). Group means calculated from the percentage of $VSV^+/NPC1^+/PLA^+$ vesicles were compared by Cohen's *d* effect size. (B) Cells described in panel A were exposed to VSV mNG-P EBOV GP uptake for 1 h at 37°C. After fixation, viral particles, NPC1, and GP_{CL} were visualized by fluorescence microscopy. Representative images from two independent experiments are shown. (C) VSV mNG-P particles bearing EBOV GP were treated *in vitro* with thermolysin (THL) or cathepsin L (CatL), respectively. Viral particles were taken up into $U2OS^{NPC1\text{-}eBFP2}$ cells followed by fixing of the cells and subjecting them to PLA. Data points represent the percentage of $VSV^+/NPC1^+/PLA^+$ compartments per individual cell; bars depict the average ± SD for all data points pooled from two independent experiments ($n \geq 25$). To compare $VSV^+/NPC1^+/PLA^+$ compartments of cells which endocytosed VSV studded with either uncleaved or THL/CatL-cleaved GP, an unpaired two-tailed *t* test was used (****, $P < 0.0001$). Cohen's *d* effect size was used to compare the group means calculated from the percentages of $VSV^+/NPC1^+/PLA^+$ vesicles ($d > 1.3$). (D) $U2OS^{NPC1\text{-}eBFP2}$ cells were (not) preincubated with E-64d (as described in panel A), and VSV mNG-P particles bearing EBOV GP were treated *in vitro* with THL. Following virus internalization into $U2OS^{NPC1\text{-}eBFP2}$, cells were fixed and subjected to PLA. Data points represent the percentage of $VSV^+/NPC1^+/PLA^+$ compartments per individual cell; bars depict the average ± SD for all data points pooled from two independent experiments ($n \geq 25$). Points with reduced transparency represent values outside the 10th to 90th percentiles. To compare $VSV^+/NPC1^+/PLA^+$ compartments of E-64d-treated cells with those of untreated cells which endocytosed VSV studded with either uncleaved or THL-cleaved GP, an unpaired two-tailed *t* test was used (**, $P < 0.01$; ***, $P < 0.001$; ****, $P < 0.0001$). Cohen's *d* effect size was used to compare the group means calculated from the percentages of $VSV^+/NPC1^+/PLA^+$ vesicles.

Previous work identified a variety of antibodies with neutralizing activity against EBOV. Those displaying exceptional neutralizing potency were described to target conformational epitopes located in the base subdomain of the GP trimeric complex (28–32). It was proposed that these base-binding antibodies efficiently block fusogenic

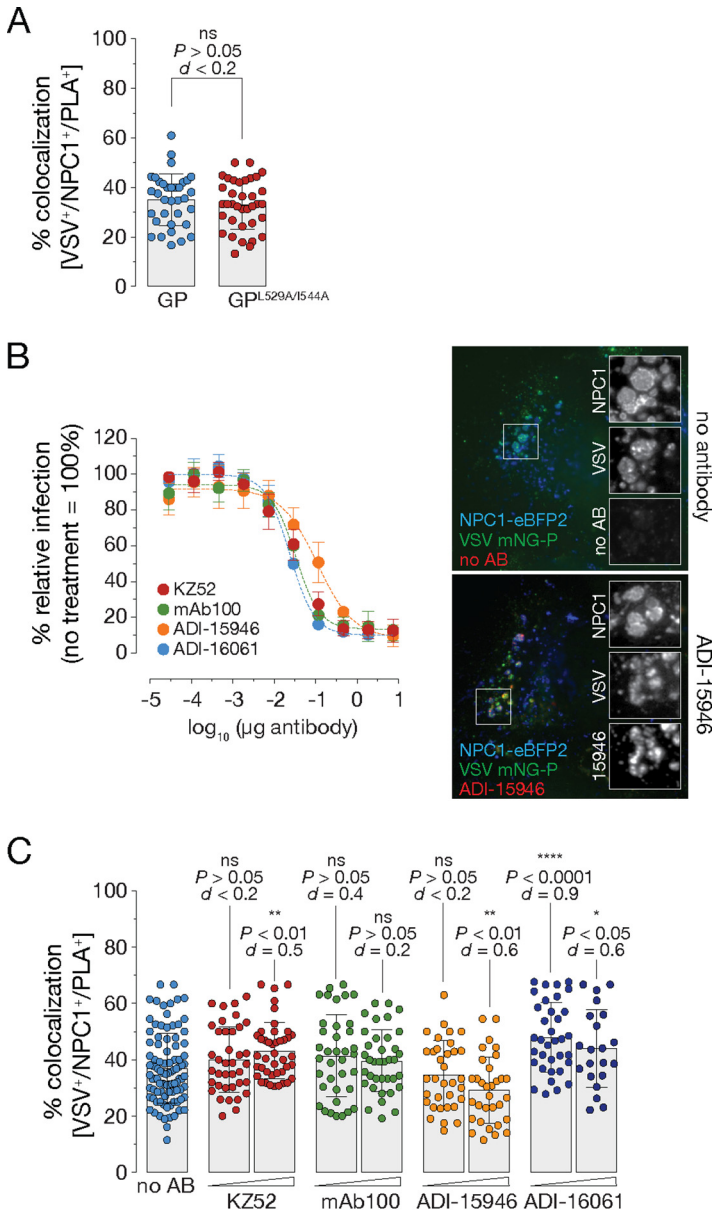

FIG 4 *In situ* proximity ligation decouples GP_{CL}-NPC1 interaction from post-binding entry steps. (A) VSV mNG-P particles bearing EBOV GP or EBOV $GP^{L529A/I544A}$ were internalized into $U2OS^{NPC1\text{-}eBFP2}$ cells for 60 min followed by PLA. Data points represent the percentage of triple-positive compartments per individual cell; bars depict the average ± SD for all data points pooled from two independent experiments ($n \geq 37$). Data analyses included an unpaired two-tailed *t* test to compare $VSV^+/NPC1^+/PLA^+$ vesicles of cells which internalized VSV decorated with wild-type or mutant GP (ns, $P > 0.05$). Cohen's *d* effect size was used to compare the group means calculated from the percentages of $VSV^+/NPC1^+/PLA^+$ compartments. (B) ADI-15946 was incubated with VSV EBOV GP particles and exposed to $U2OS^{NPC1\text{-}eBFP2}$ (right). After virus uptake for 1 h at 37°C, cells were fixed, and viral particles, NPC1, and bound antibodies were visualized by fluorescence microscopy. Representative images from two independent experiments are shown. Virions were preincubated with increasing amounts of KZ52, mAb100, ADI-15946, or ADI-16061 and then exposed to $U2OS^{NPC1\text{-}eBFP2}$ cells for 16 h at 37°C (left). The number of infected cells was determined by automated counting of mNG^+ cells and normalized to infection obtained in the absence of antibodies. Averages ± SD for six technical replicates pooled from two independent experiments are shown. (C) VSV mNG-P EBOV GP virions were complexed with KZ52, mAb100, ADI-15946, or ADI-16061 (50 μg/ml and 100 μg/ml) for 1 h at room temperature. Following internalization into $U2OS^{NPC1\text{-}eBFP2}$, cells were fixed and subjected to *in situ* PLA. Data points represent the percentage of $VSV^+/NPC1^+/PLA^+$ compartments per individual cell; bars show the average ± SD for all data points pooled from two independent experiments ($n \geq 22$). $VSV^+/NPC1^+/PLA^+$ vesicles were analyzed by unpaired two-tailed *t* test (ns, $P > 0.05$; *, $P < 0.05$; **, $P < 0.01$; ****, $P < 0.0001$) comparing cells which were exposed to virion-antibody complexes to cells exposed to untreated virus. Group means calculated from the percentage of $VSV^+/NPC1^+/PLA^+$ vesicles were also compared by Cohen's *d* effect size.

rearrangements of GP, thereby inhibiting viral entry steps downstream of NPC1 binding. We used these neutralizing antibodies to further investigate if *in situ* PLA monitored GP_{CL}-NPC1 binding specifically or also integrated post-receptor binding events (e.g., viral membrane fusion). We tested antibodies targeting the GP_1-GP_2 interface (KZ52, mAb100), the GP_1-GP_2 interface plus the glycan cap (ADI-15946), or a subdomain of the fusion loop, the heptad repeat 2 (ADI-16061). Preincubation of VSVs with these neutralizing antibodies (50 μg/ml) afforded delivery of virus-antibody complexes to $NPC1^+$ LE but did not hinder virus trafficking to LEs itself or proteolytic processing to GP_{CL} (Fig. 4B, right, and Fig. S5B and C). However, infection was blocked under these conditions, as expected (Fig. 4B, left). Despite their potent neutralizing activity, and consistent with the specified target epitopes as well as previously reported *in vitro* NPC1-binding studies (28–32), base-binding antibodies mAb100 and ADI-15946 had little or no effect on *in situ* PLA, consistent with our hypothesis that this assay selectively detects GP_{CL}-NPC1 complex formation (Fig. 4C). Surprisingly, incubation with KZ52 and ADI-16061 slightly improved the PLA signal, possibly because they enhanced an upstream step, the delivery of VSV bearing GP_{CL} to $NPC1^+$ LE (Fig. 4C).

Collectively, our results provide strong evidence that the *in situ* PLA specifically monitors GP_{CL}-NPC1 binding in infected cells and decouples the detection of virus-receptor binding from post-receptor binding steps in viral entry.

Small-molecule inhibitor-mediated selective interference of GP-NPC1 binding delineated by *in situ* PLA. The unprecedented EBOV outbreak in West Africa from 2013 to 2016 uncovered a pressing need for anti-EBOV therapeutics; since then, numerous studies screened for and characterized FDA-approved drugs with anti-filoviral activity. The most promising drug candidates, amiodarone, bepridil, clomifene, sertraline, and toremifene, were reported to block one or several steps during EBOV entry (15, 33–39). As their precise mechanisms of anti-EBOV activity still remain elusive, we examined the capacity of these inhibitors to alter intracellular GP_{CL}-NPC1 interaction in the PLA. As a control, we also tested the well-characterized amphiphilic drug U18666A, which was described to block cholesterol export from lysosomes and shown to inhibit EBOV entry at higher concentrations, but not to impact GP_{CL}-NPC1 binding *in vitro* (9, 15, 40).

We first titrated the drugs in an EBOV entry assay in wild-type U2OS and $U2OS^{NPC1\text{-}eBFP2}$ cells overexpressing NPC1 employed in the PLA (Fig. 5A and Fig. S6A). Several of the inhibitors were less potent in NPC1-overexpressing cells than in wild-type cells, as reported previously, suggesting they act via the GP_{CL}-NPC1 axis (15) (Fig. S6A). Some inhibitors hampered VSV trafficking to $NPC1^+$ LE, whereas others had little or no effect on viral delivery to $NPC1^+$ LE compared to a dimethyl sulfoxide (DMSO)-treated control (Fig. S6B). Because these trafficking defects likely contribute to the observed inhibition in infection, we sought to discount these trafficking effects on GP_{CL}-NPC1 binding by focusing exclusively on PLA activity in $VSV^+/NPC1^+$ compartments. Importantly, these inhibitors exhibited little or no effect on GP cleavage (detected by MR72) or the accessibility of NPC1 domain C (detected by MAb-548) (Fig. 5C; data not shown).

Screening the inhibitory compounds via PLA revealed that amiodarone, bepridil, clomifene, sertraline, and toremifene all significantly interfered with GP_{CL}-NPC1 interaction compared to a DMSO-treated control (Fig. 5B). In contrast, but consistent with previous *in vitro* data, U18666A did not block GP_{CL}-NPC1 binding (Fig. 5B). The drug treatments also substantially modified NPC1 trafficking to LE and/or LE localization; we observed pronounced imbalances in NPC1 distribution, illustrated by LE vesicles with extensively elevated or decreased NPC1 levels accumulating in the perinuclear regions of cells (Fig. 5C and Fig. S6C, bottom). Further, NPC1's transporter activity was strongly impaired; although cells did not exhibit cholesterol accumulation in $NPC1^+$ LE following the short-term drug treatments carried out prior to PLA measurements, prolonged inhibitor incubations (16 h instead of 1 h of incubation prior to PLA) clearly blocked cholesterol clearance from LE (Fig. 5C and Fig. S6C, top).

In summary, our results imply that a number of FDA-approved small-molecule inhibitors interfere with GP_{CL}-NPC1 engagement, and such block downstream viral

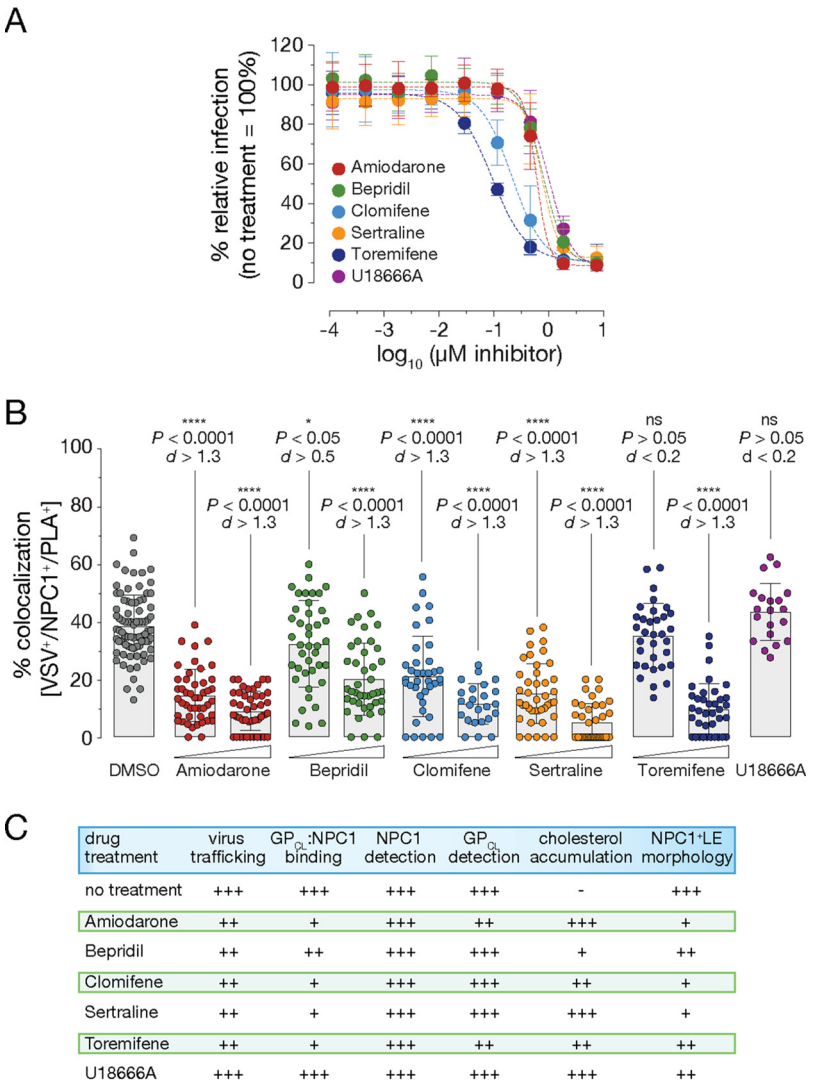

C

drug treatment	virus trafficking	GP_{CL}:NPC1 binding	NPC1 detection	GP_{CL} detection	cholesterol accumulation	$NPC1^+$LE morphology
no treatment	+++	+++	+++	+++	-	+++
Amiodarone	++	+	+++	++	+++	+
Bepridil	++	++	+++	+++	+	++
Clomifene	++	+	+++	+++	++	+
Sertraline	++	+	+++	+++	+++	+
Toremifene	++	+	+++	++	++	++
U18666A	+++	+++	+++	+++	+++	++

FIG 5 Small-molecule inhibitor-mediated selective interference of GP-NPC1 binding delineated by *in situ* PLA. (A) $U2OS^{NPC1\text{-}eBFP2}$ cells were preincubated with increasing concentrations of amiodarone, bepridil, clomifene, sertraline, toremifene, and U18666A, respectively, before exposure to VSV mNG-P EBOV GP for 16 h at 37°C. Infection was measured by automated counting of mNG^+ cells and normalized to infection obtained in the presence of vehicle only. Averages ± SD for 9 to 18 technical replicates pooled from 3 to 6 independent experiments are displayed. (B) $U2OS^{NPC1\text{-}eBFP2}$ cells were incubated with amiodarone, bepridil, clomifene, and sertraline, respectively (2 μM or 5 μM, 1 h at 37°C), toremifene (2 μM or 10 μM, 1 h at 37°C), or U18666A (10 μM, 2 h at 37°C), followed by VSV mNG-P EBOV GP uptake for 1 h. Cells were subjected to *in situ* PLA and analyzed by fluorescence microscopy. The percentage of triple-positive $VSV^+/NPC1^+/PLA^+$ compartments per individual cell is represented by data points; bars show the average ± SD for all data points pooled from two independent experiments ($n \geq 20$). $VSV^+/NPC1^+/PLA^+$ vesicles were analyzed by unpaired two-tailed *t* test (ns, $P > 0.05$; *, $P < 0.05$; ****, $P < 0.0001$) comparing inhibitor-exposed to untreated cells. Group means calculated from the percentage of $VSV^+/NPC1^+/PLA^+$ compartments were also compared by Cohen's *d* effect size. (C) Table summarizing results from panel B and Fig. S6 in the supplemental material. Data for "virus trafficking" can be found in Fig. S6B, data for "GP_{CL}-NPC1 binding" are shown in panel B, data for "NPC1 detection" and "GP_{CL} detection" are not shown, exemplary images for "cholesterol accumulation" are depicted in Fig. S6C, top, and exemplary images for "$NPC1^+$ LE morphology" are shown in Fig. S6C, bottom.

entry steps. However, our findings and previously published work indicate that the inhibitory mode of action of these compounds is likely multifactorial. Although our data suggest that some of the compounds directly affect GP_{CL}-NPC1 interaction in endosomal compartments during entry, they also uncover contributions from drug-induced changes in the morphology and distribution of $NPC1^+$ compartments.

DISCUSSION

Interaction of the filovirus spike protein GP with its universal intracellular receptor NPC1 is indispensable for viral entry and infection (9–13). However, our understanding of the mechanism of GP-NPC1 recognition is largely derived from *in vitro* assays that use detergent-extracted NPC1 or a soluble form of the GP-interacting domain C of NPC1 together with *in vitro*-cleaved GP_{CL} (10, 11). Although powerful, these assays likely do not fully recapitulate the authentic virus-receptor interaction in late endo-/lysosomal compartments. As a case in point, a number of small-molecule entry inhibitors that appear to target NPC1 in cells do not block GP_{CL}-NPC1 domain C interaction *in vitro*, leaving open questions about their mechanism of action (15).

Here, we describe a novel assay that monitors the GP-NPC1 interaction in intact cells. Detection of virus-receptor complexes *in situ* is based on the principle of DNA-assisted, antibody-mediated proximity ligation (20, 21). Several studies have used PLAs to detect interaction of virus particles with host proteins at the plasma membrane (41), in the cytoplasm (42, 43), and in early endosomes (44). To our knowledge, our assay represents the first example to afford visualization of protein-protein interactions in late endosomal/lysosomal compartments.

Previous studies used *in vitro* protease treatments in conjunction with infectivity measurements in protease inhibitor-treated or genetically engineered cells to establish a requirement for GP cleavage in EBOV entry (6–8). Further, *in vitro* binding studies with soluble NPC1 domains demonstrated that GP cleavage is required for virus-receptor interaction (9–13). Here, we used the PLA to directly investigate the role of GP proteolytic cleavage in GP-NPC1 interaction within cellular endo-/lysosomal compartments. Concordant with our current understanding, we found that blockade of all endosomal cysteine cathepsins with the pan-cysteine cathepsin inhibitor E-64d abrogated both GP cleavage and GP-NPC1 association *in situ* and that *in vitro* pre-cleavage of EBOV GP to GP_{CL} significantly boosted this interaction. We also observed that genetic knockout of the two key cysteine cathepsins identified previously, CatB and CatL, substantially inhibited GP-NPC1 association as measured by PLA. Unexpectedly, knocking out *CatB* and *CatL* did not prevent exposure of the RBS in endosomes, as judged by the continued capacity of RBS-specific MAb MR72 to detect viral particles. Thus, one or more non-CatB/CatL cysteine cathepsins appear to at least partially cleave GP in endosomes in a manner that, however, does not permit stable GP-NPC1 association. Alternatively, it is possible that CatB and/or CatL mediate additional yet undiscovered cleavage events that are required for GP-NPC1 binding.

Similar to published *in vitro* GP-NPC1 binding assays, our *in situ* PLA could also specifically detect GP-NPC1 interactions independent of downstream post-binding steps in entry, allowing us to focus on molecular mechanisms underlying the receptor-binding step. We employed fusion-blocking GP mutants and neutralizing antibodies targeting epitopes essential for GP's conformational rearrangements during membrane fusion; both interventions, however, left GP_{CL}-NPC1 binding measured by PLA largely unaffected. Previous publications suggested a dual mechanism of action for several of these antibodies, KZ52, mAb100, and ADI-15946 (28, 30); to block EBOV GP-mediated infection, they hampered post-NPC1-binding steps and interfered with GP's proteolytic processing *in vitro*. Surprisingly, the latter *in vitro* findings were not recapitulated by the *in situ* PLA. Our results suggest that in the presence of neutralizing antibodies, the CatB/L cleavage sites located in GP's β13-β14 loop were readily accessible in an *in situ* endosomal environment, while they did not appear to be in the *in vitro* cell-free system. Potential minor changes in the GP cleavage efficiency cannot be monitored via the RBS-specific MAb MR72; however, our PLA results suggest that the level of GP cleavage was sufficient to allow efficient NPC1 binding. Further, our experiments suggest that *in vitro* cleavage studies do not fully recapitulate the authentic interactions

within the trifecta of endosomal proteases, virus glycoproteins, and GP-targeting MAbs in an acidic endosomal environment.

Lastly, by examining the effect of small-molecule inhibitors on GP_{CL}-NPC1 binding, we further unraveled their multifaceted mechanisms of inhibitory action toward EBOV GP-mediated infection. All FDA-approved drugs tested, amiodarone, bepridil, clomifene, sertraline, and toremifene, significantly hampered GP_{CL}-NPC1 interaction measured by *in situ* PLA. Previous reports focused on bepridil, sertraline, and toremifene, which were proposed to destabilize GP's prefusion conformation by binding into a cavity at the GP_1-GP_2 interface *in silico* and *in vitro* (35, 38, 39). Our data also indicated changes in the intracellular distribution and morphology of $NPC1^+$ LE/LY, as well as NPC1's cholesterol transporter function following drug incubations. This was most notable for toremifene, clomifene, and sertraline, suggesting that they (in addition) also acted via the GP_{CL}-NPC1 axis; overexpression of NPC1 clearly counteracted their inhibitory mechanism during infection. We propose that the loss of GP_{CL}-NPC1 binding is most likely caused by adverse effects on both NPC1 and GP, leading to destabilization of GP and drastic modifications in the $NPC1^+$ LE/LY phenotype. Resolving the effects of small-molecule inhibitors on GP_{CL}-NPC1 binding remains the focus of ongoing work and will help us to decode this interaction in more detail.

In summary, the newly established *in situ* proximity ligation assay provides a powerful new tool to delineate molecular mechanisms underlying receptor-filoviral glycoprotein interactions, to characterize host factors modulating EBOV entry, to unravel the mode of action of antibodies and small-molecule inhibitors, and to explore yet unidentified host proteins and their ability to affect formation of the multivalent GP_{CL}-NPC1 interface in a cell-based system. In principle, it is also feasible that unknown host factors within the endosomal milieu might participate in establishing GP_{CL}-NPC1 binding; we suggest that our *in situ* proximity ligation assay may aid in the identification of such entry host factors.

MATERIALS AND METHODS

Cells and viruses. Human osteosarcoma U2OS cells were cultured in modified McCoy's 5A medium (Life Technologies) supplemented with 10% fetal bovine serum (Atlanta Biologicals), 1% penicillin-streptomycin (Life Technologies), and 1% GlutaMax (Life Technologies). Cells were kept at 37°C with 5% CO_2 in a humidified incubator. U2OS cells stably overexpressing NPC1-eBFP2 were generated as described previously and maintained under the same conditions mentioned above (16). Propagation of recombinant vesicular stomatitis Indiana virus (rVSV) expressing enhanced green fluorescent protein (eGFP) in the first position and bearing the VSV G or EBOV GP glycoprotein, derived from EBOV/H.sap/COD/76/Yam-Mayinga (EBOV "Mayinga" isolate) as well as an rVSV bearing the EBOV GP glycoprotein, and a monomeric NeonGreen-phosphoprotein P (mNG-P) fusion protein has been described previously (4, 45–47). Pseudotyped VSVs bearing mNG-P and variant GPs, $GP^{T83M/K114E/K115E}$ and $GP^{L529A/I544A}$ (both also lacking the mucin-like domain), were prepared as previously reported (6, 24, 48).

For some experiments, cleaved viral particles bearing GP_{CL} were first generated by incubation with thermolysin (THL; 1 mg/ml, pH 7.5, 37°C for 1 h; Sigma) or recombinant human cathepsin L (CatL, 2 ng/μl, pH 5.5, 37°C for 1 h; R&D Systems) as described previously (4). Reactions were stopped by removal onto ice and addition of phosphoramidon (1 mM; Peptides International) or E-64 (10 μm; Peptides International), respectively. While viral particles cleaved with CatL were used immediately, THL-cleaved virus was kept at −80°C until usage.

Antibodies. For immunofluorescence analysis, NPC1-eBFP2 was detected by a rabbit anti-BFP antibody (GeneTex) followed by a secondary anti-rabbit antibody -Alexa 405 or -Alexa 488 fluorophore (Thermo Scientific). During proximity ligation assay (PLA), NPC1 was detected by MAb-548, whose generation was described earlier (16). Detection of proteolytically cleaved GP was carried out with an RBS-specific human anti-GP antibody, MR72, either followed by a secondary anti-human antibody-Alexa 555 fluorophore or following the PLA protocol as described below. To detect EBOV GP by immunofluorescence analysis and to determine the effect of GP-targeting antibodies on GP_{CL}-NPC1 interaction, we used the previously described human anti-GP antibodies KZ52, MAb100, ADI-15946, and ADI-16061 (28–32). For production of KZ52, ADI-15946, and ADI-16061, variable heavy- and light-chain domain sequences were cloned into the mammalian expression vectors pMAZ-IgL (encoding the expression cassette of human κ light-chain constant domains) and pMAZ-IgH (encoding the expression cassette of human γ1 chain constant domains). Antibody production in FreeStyle 293-F cells (Thermo Fisher) and subsequent purification were carried out as described earlier (16).

Inhibitors. Stock solutions of drugs were prepared in dimethyl sulfoxide (DMSO) and stored as frozen aliquots until use. Cells were incubated with 3.47 (Microbiotix), amiodarone (Sigma), bepridil (Sigma), clomifene (Sigma), sertraline (Toronto Research Chemicals), or toremifene (Sigma) for 1 h or

16 h at 37°C with concentrations as indicated. Incubation of cells with E-64d (Peptides International) was extended to 6 h at 37°C, while cells were not preincubated with U18666A (Calbiochem) for PLA, but preincubated for 1 h or 16 h at 37°C for additional described experiments at concentrations indicated. Inhibitors were maintained at the same concentrations during virus spinoculation and virus entry into cells.

Generation of U2OS *CatB/L* double-knockout cells overexpressing NPC1. U2OS cells were transduced with a lentivirus carrying human codon-optimized *Streptomyces pyogenes* Cas9 (spCas9) and blasticidin resistance genes to generate U2OS-Cas9 cells expressing Cas9. Briefly, 293FT cells were cotransfected with Cas9-expressing plasmid lentiCas9-BLAST (Addgene plasmid no. 52962, a gift from Feng Zhang), the lentiviral packaging plasmid psPAX2 (Addgene plasmid no. 12260, a gift from Didier Trono), and a VSV G-expressing plasmid. The supernatant filtered through a 0.45-μm filter was used to transduce U2OS cells in the presence of 6 μg/ml of polybrene, and transduced cells were selected with 15 μg/ml of blasticidin. A lentiGuide-Puro plasmid (Addgene plasmid no. 52963, a gift from Feng Zhang) expressing human *CatL*-targeting sgRNA (5′-CTTAGGGATGTCCACAAAGC-3′; targets anti-sense strand, nucleotides (nt) 1,021 to 1,040 of the *CatL* transcript variant 1 mRNA or nt 4,205 to 4,186 of *CatL*, NCBI gene ID 1514) was used to generate lentiviruses as described above. U2OS-Cas9 cells transduced with these lentiviruses were selected with 2 μg/ml of puromycin. Editing of the *CatL* gene was confirmed by Sanger sequencing of a 673-bp amplicon using primers flanking the single guide RNA (sgRNA) target site. A single cell clone carrying a homozygous deletion of 15 nucleotides that is predicted to disrupt a critical N-glycosylation site (204-NDT-206) that is required for lysosomal targeting of CatL by causing a T206I change (along with a deletion of amino acids [aa] 207 to 210) was selected (49, 50). Absence of wild-type allele from the *CatL* knockout (KO) cells was confirmed by reverse transcriptase PCR (RT-PCR) using primers specific for the 15-nt deletion. To generate the *CatB/L* double KO, the *CatL*-KO cells were further transduced with a lentivirus encoding *CatB*-specific sgRNA (5′-TTGACCAGCTCATCCGACAG-3′; targets anti-sense strand, nt 251 to 270 of human *CatB* transcript variant 1 mRNA or nt 14,791 to 14,772 of human *CatB*, NCBI gene ID 1508). A single cell clone carrying an insertion of a single nucleotide (T) that is predicted to cause a frameshift leading to a truncated propeptide of 28 amino acids (frameshift at aa position 27) was selected. Absence of *CatB* and *CatL* activity in this single-cell clone was confirmed by cathepsin activity assays (described below). Stable U2OS cells expressing NPC1 C-terminally tagged with a triple flag sequence in the *CatB/L*-KO background were generated as described earlier. In short, retroviruses packaging the transgene were produced by triple transfection of 293T cells, and target U2OS cells were directly exposed to sterile-filtered retrovirus-laden supernatants in the presence of polybrene (6 μg/ml). Transduced cell populations were selected with puromycin (2 μg/ml), and expression of Flag-tagged NPC1 was confirmed by immunostaining with an anti-Flag M2 antibody (Sigma).

Cathepsin L and B activity assay. U2OS-Cas9, U2OS *CatL*-KO, U2OS *CatB*-KO, and U2OS *CatB/L*-KO cells stably expressing Flag-tagged NPC1 were lysed (50 mM morpholineethanesulfonic acid [MES] [pH 5.5], 135 mM NaCl, 2 mM ethylenediaminetetraacetic acid [EDTA], and 0.5% Triton X-100) for 1 h on ice. As a control, cleared U2OS-Cas9 lysates were preincubated with the protease inhibitor E-64 (20 μM; Peptides International) for 20 min at room temperature (when indicated). Then, lysates were mixed with reaction buffer (100 mM Na acetate [pH 5], 1 mM EDTA, and 4 mM dithiothreitol), incubated with the fluorogenic peptide substrate Z-FR-AMC (150 μM; R&D Systems), and measured at a fluorometer following a 0- to 30-min incubation (excitation wavelength [λ_{ex}], 390 nm; emission wavelength [λ_{em}], 460 nm). Measurements of substrate hydrolysis were normalized to maximum hydrolysis on U2OS-Cas9 cells reached after 30 min; data represent the mean value and standard deviations of three independent experiments ($n = 3$).

Infection experiments. Confluent U2OS cells were infected with pre-titrated amounts of pseudotyped VSV particles bearing wild-type or mutant GPs. Prior to infection, VSVs were diluted in corresponding media, and infected cells were maintained at 37°C for 14 to 16 h post-infection before manual counting of $eGFP^+$ and mNG^+ cells or automated counting using a Cytation 5 cell imaging multimode reader (BioTek Instruments) and a CellInsight CX5 imager (Thermo Fisher) including onboard software. When indicated, cells were preincubated with small-molecule inhibitors diluted in corresponding media; for antibody neutralization experiments, VSV particles were incubated with increasing concentrations of test antibodies at room temperature for 1 h prior to addition to cell monolayers. Virus infectivities were measured as described above. Virus neutralization data were subjected to nonlinear regression analysis (4-parameter, variable slope sigmoidal dose-response equation; GraphPad Prism).

Immunofluorescence microscopy and immunostaining. To investigate determinants of VSV mNG-P EBOV GP internalization into endosomal compartments, pre-titrated amounts of VSV particles bearing mNG-P and either wild-type or mutant EBOV GP were diluted into imaging buffer (20 mM HEPES [pH 7.4], 140 mM NaCl, 2.5 mM KCl, 1.8 mM $CaCl_2$, 1 mM $MgCl_2$, 5 mM glucose, and 2% fetal bovine serum [FBS]) and spinoculated onto prechilled $U2OS^{NPC1\text{-}eBFP2}$ cells on coverslips. Unbound virus was removed by washing with cold phosphate-buffered saline (PBS). Cells were then placed in warm imaging buffer and allowed to internalize VSVs for 1 h at 37°C. Cells were fixed with 3.7% paraformaldehyde and permeabilized with PBS/0.1% Triton X-100. NPC1-eBFP2 was detected with either primary mouse anti-NPC1 MAb-548 or rabbit anti-BFP antibodies and secondary anti-mouse or anti-rabbit antibody-Alexa 405 fluorophore conjugates, respectively (Thermo Scientific). Cleaved GP was detected with the primary mouse RBS-specific anti-GP antibody MR72 followed by secondary anti-mouse antibody-Alexa 555 fluorophore conjugate (Thermo Scientific). To investigate transport of IgGs bound to VSV particles into $NPC1^+$ endosomal compartments, VSV particles bearing mNG-P were preincubated with antibodies (50 or 100 μg/ml, respectively) for 1 h at room temperature, followed by internalization into target cells and detection by incubation with secondary anti-human-Alexa 555 fluorophore conjugates (Thermo Scientific). Cells were examined by immunofluorescence analysis performed on an Axio Observer Z1 widefield

epifluorescence microscope (Zeiss Inc.) equipped with an ORCA-Flash4.0 LT digital CMOS (complementary metal oxide semiconductor) camera (Hamamatsu Photonics), a 63×, 1.4 numerical aperture oil immersion objective, and a DAPI (4′,6-diamidino-2-phenylindole)/fluorescein isothiocyanate (FITC)/tetramethyl rhodamine isocyanate (TRITC)/Cy5 filter set. Images were processed in Photoshop (Adobe Systems).

Cholesterol accumulation assay. Cholesterol accumulation following inhibitor treatment of U2OS$^{NPC1\text{-}eBFP2}$ cells was monitored by incubation with filipin (50 μg/ml; Sigma) for 1 h at room temperature. Cells were examined by immunofluorescence analysis as described in the Materials and Methods section "Immunofluorescence microscopy and immunostaining."

Proximity ligation assay. U2OS$^{NPC1\text{-}eBFP2}$ cells were allowed to internalize VSV particles (in the presence or absence of small-molecule inhibitors or antibodies), fixed, and permeabilized as described in the Materials and Methods section "Immunofluorescence microscopy and immunostaining." MR72, an RBS-targeting anti-GP MAb, and MAb-548, an NPC1 domain C-targeting MAb, were directly labeled with Duolink In Situ Probemaker Plus and Duolink In Situ Probemaker Minus (Sigma) following the manufacturer's instructions. Fixed cells were incubated with labeled antibodies in a humidity chamber at 37°C for 1 h. Excess antibody was removed by washing with Duolink in situ wash buffer (Sigma). GP-NPC1 interaction was detected by applying the Duolink in situ detection reagents red kit following the manufacturer's instructions (Sigma). After removing excess reagents, NPC1-eBFP2 was detected using a rabbit anti-BFP antibody followed by a secondary anti-rabbit antibody-Alexa 405 fluorophore conjugate (Thermo Fisher). Cells were examined by immunofluorescence analysis as described in the Materials and Methods section "Immunofluorescence microscopy and immunostaining."

SUPPLEMENTAL MATERIAL

Supplemental material is available online only.

FIG S1, TIF file, 2.4 MB.

FIG S2, TIF file, 2.1 MB.

FIG S3, TIF file, 0.2 MB.

FIG S4, TIF file, 0.5 MB.

FIG S5, TIF file, 1.2 MB.

FIG S6, TIF file, 1.5 MB.

ACKNOWLEDGMENTS

We acknowledge Isabel Gutierrez, Estefania Valencia, Laura Polanco, and Cecelia Harold for laboratory management and technical support.

This work was supported by National Institutes of Health (NIH) grant R01AI134824 (to K.C.).

K.C. is a member of the Scientific Advisory Board of Integrum Scientific, LLC.

REFERENCES

1. Feldmann H, Geisbert TW. 2011. Ebola haemorrhagic fever. Lancet 377:849–862. https://doi.org/10.1016/S0140-6736(10)60667-8.
2. Saeed MF, Kolokoltsov AA, Albrecht T, Davey RA. 2010. Cellular entry of Ebola virus involves uptake by a macropinocytosis-like mechanism and subsequent trafficking through early and late endosomes. PLoS Pathog 6:e1001110. https://doi.org/10.1371/journal.ppat.1001110.
3. Mulherkar N, Raaben M, de la Torre JC, Whelan SP, Chandran K. 2011. The Ebola virus glycoprotein mediates entry via a non-classical dynamin-dependent macropinocytic pathway. Virology 419:72–83. https://doi.org/10.1016/j.virol.2011.08.009.
4. Spence JS, Krause TB, Mittler E, Jangra RK, Chandran K. 2016. Direct visualization of Ebola virus fusion triggering in the endocytic pathway. mBio 7:e01857-15. https://doi.org/10.1128/mBio.01857-15.
5. Nanbo A, Imai M, Watanabe S, Noda T, Takahashi K, Neumann G, Halfmann P, Kawaoka Y. 2010. Ebolavirus is internalized into host cells via macropinocytosis in a viral glycoprotein-dependent manner. PLoS Pathog 6:e1001121. https://doi.org/10.1371/journal.ppat.1001121.
6. Chandran K, Sullivan NJ, Felbor U, Whelan SP, Cunningham JM. 2005. Endosomal proteolysis of the Ebola virus glycoprotein is necessary for infection. Science 308:1643–1645. https://doi.org/10.1126/science.1110656.
7. Schornberg K, Matsuyama S, Kabsch K, Delos S, Bouton A, White J. 2006. Role of endosomal cathepsins in entry mediated by the Ebola virus glycoprotein. J Virol 80:4174–4178. https://doi.org/10.1128/JVI.80.8.4174-4178.2006.
8. Misasi J, Chandran K, Yang J-Y, Considine B, Filone CM, Côté M, Sullivan N, Fabozzi G, Hensley L, Cunningham J. 2012. Filoviruses require endosomal cysteine proteases for entry but exhibit distinct protease preferences. J Virol 86:3284–3292. https://doi.org/10.1128/JVI.06346-11.
9. Carette JE, Raaben M, Wong AC, Herbert AS, Obernosterer G, Mulherkar N, Kuehne AI, Kranzusch PJ, Griffin AM, Ruthel G, Dal Cin P, Dye JM, Whelan SP, Chandran K, Brummelkamp TR. 2011. Ebola virus entry requires the cholesterol transporter Niemann-Pick C1. Nature 477:340–343. https://doi.org/10.1038/nature10348.
10. Miller EH, Obernosterer G, Raaben M, Herbert AS, Deffieu MS, Krishnan A, Ndungo E, Sandesara RG, Carette JE, Kuehne AI, Ruthel G, Pfeffer SR, Dye JM, Whelan SP, Brummelkamp TR, Chandran K. 2012. Ebola virus entry requires the host-programmed recognition of an intracellular receptor. EMBO J 31:1947–1960. https://doi.org/10.1038/emboj.2012.53.
11. Côté M, Misasi J, Ren T, Bruchez A, Lee K, Filone CM, Hensley L, Li Q, Ory D, Chandran K, Cunningham J. 2011. Small molecule inhibitors reveal Niemann-Pick C1 is essential for Ebola virus infection. Nature 477:344–348. https://doi.org/10.1038/nature10380.
12. Ng M, Ndungo E, Jangra RK, Cai Y, Postnikova E, Radoshitzky SR, Dye JM, Ramírez de Arellano E, Negredo A, Palacios G, Kuhn JH, Chandran K. 2014. Cell entry by a novel European filovirus requires host endosomal cysteine proteases and Niemann-Pick C1. Virology 468–470:637–646. https://doi.org/10.1016/j.virol.2014.08.019.
13. Goldstein T, Anthony SJ, Gbakima A, Bird BH, Bangura J, Tremeau-Bravard A, Belaganahalli MN, Wells HL, Dhanota JK, Liang E, Grodus M, Jangra RK, DeJesus VA, Lasso G, Smith BR, Jambai A, Kamara BO, Kamara S, Bangura W, Monagin C, Shapira S, Johnson CK, Saylors K, Rubin EM, Chandran K, Lipkin WI, Mazet JAK. 2018. The discovery of Bombali virus adds further support for bats as hosts of ebolaviruses. Nat Microbiol 3:1084–1089. https://doi.org/10.1038/s41564-018-0227-2.
14. Bale S, Liu T, Li S, Wang Y, Abelson D, Fusco M, Woods VL, Saphire EO.

2011. Ebola virus glycoprotein needs an additional trigger, beyond proteolytic priming for membrane fusion. PLoS Negl Trop Dis 5:e1395. https://doi.org/10.1371/journal.pntd.0001395.
15. Shoemaker CJ, Schornberg KL, Delos SE, Scully C, Pajouhesh H, Olinger GG, Johansen LM, White JM. 2013. Multiple cationic amphiphiles induce a Niemann-Pick C phenotype and inhibit Ebola virus entry and infection. PLoS One 8:e56265. https://doi.org/10.1371/journal.pone.0056265.
16. Wec AZ, Nyakatura EK, Herbert AS, Howell KA, Holtsberg FW, Bakken RR, Mittler E, Christin JR, Shulenin S, Jangra RK, Bharrhan S, Kuehne AI, Bornholdt ZA, Flyak AI, Saphire EO, Crowe JE, Aman MJ, Dye JM, Lai JR, Chandran K. 2016. A "Trojan horse" bispecific-antibody strategy for broad protection against ebolaviruses. Science 354:350–354. https://doi.org/10.1126/science.aag3267.
17. Bornholdt ZA, Ndungo E, Fusco ML, Bale S, Flyak AI, Crowe JE, Chandran K, Saphire EO. 2016. Host-primed Ebola virus GP exposes a hydrophobic NPC1 receptor-binding pocket, revealing a target for broadly neutralizing antibodies. mBio 7:e02154-15. https://doi.org/10.1128/mBio.02154-15.
18. Flyak AI, Ilinykh PA, Murin CD, Garron T, Shen X, Fusco ML, Hashiguchi T, Bornholdt ZA, Slaughter JC, Sapparapu G, Klages C, Ksiazek TG, Ward AB, Saphire EO, Bukreyev A, Crowe JE. 2015. Mechanism of human antibody-mediated neutralization of Marburg virus. Cell 160:893–903. https://doi.org/10.1016/j.cell.2015.01.031.
19. Söderberg O, Leuchowius K-J, Gullberg M, Jarvius M, Weibrecht I, Larsson L-G, Landegren U. 2008. Characterizing proteins and their interactions in cells and tissues using the in situ proximity ligation assay. Methods 45:227–232. https://doi.org/10.1016/j.ymeth.2008.06.014.
20. Fredriksson S, Gullberg M, Jarvius J, Olsson C, Pietras K, Gústafsdóttir SM, Ostman A, Landegren U. 2002. Protein detection using proximity-dependent DNA ligation assays. Nat Biotechnol 20:473–477. https://doi.org/10.1038/nbt0502-473.
21. Gullberg M, Fredriksson S, Taussig M, Jarvius J, Gustafsdottir S, Landegren U. 2003. A sense of closeness: protein detection by proximity ligation. Curr Opin Biotechnol 14:82–86. https://doi.org/10.1016/s0958-1669(02)00011-3.
22. Wang H, Shi Y, Song J, Qi J, Lu G, Yan J, Gao GF. 2016. Ebola viral glycoprotein bound to its endosomal receptor Niemann-Pick C1. Cell 164:258–268. https://doi.org/10.1016/j.cell.2015.12.044.
23. Fels JM, Spence JS, Bortz RH, Bornholdt ZA, Chandran K. 2019. A hyperstabilizing mutation in the base of the Ebola virus glycoprotein acts at multiple steps to abrogate viral entry. mBio 10:e01408-19. https://doi.org/10.1128/mBio.01408-19.
24. Wong AC, Sandesara RG, Mulherkar N, Whelan SP, Chandran K. 2010. A forward genetic strategy reveals destabilizing mutations in the Ebolavirus glycoprotein that alter its protease dependence during cell entry. J Virol 84:163–175. https://doi.org/10.1128/JVI.01832-09.
25. Kaletsky RL, Simmons G, Bates P. 2007. Proteolysis of the Ebola virus glycoproteins enhances virus binding and infectivity. J Virol 81:13378–13384. https://doi.org/10.1128/JVI.01170-07.
26. Brecher M, Schornberg KL, Delos SE, Fusco ML, Saphire EO, White JM. 2012. Cathepsin cleavage potentiates the Ebola virus glycoprotein to undergo a subsequent fusion-relevant conformational change. J Virol 86:364–372. https://doi.org/10.1128/JVI.05708-11.
27. Gregory SM, Harada E, Liang B, Delos SE, White JM, Tamm LK. 2011. Structure and function of the complete internal fusion loop from Ebolavirus glycoprotein 2. Proc Natl Acad Sci U S A 108:11211–11216. https://doi.org/10.1073/pnas.1104760108.
28. Misasi J, Gilman MSA, Kanekiyo M, Gui M, Cagigi A, Mulangu S, Corti D, Ledgerwood JE, Lanzavecchia A, Cunningham J, Muyembe-Tamfun JJ, Baxa U, Graham BS, Xiang Y, Sullivan NJ, McLellan JS. 2016. Structural and molecular basis for Ebola virus neutralization by protective human antibodies. Science 351:1343–1346. https://doi.org/10.1126/science.aad6117.
29. West BR, Wec AZ, Moyer CL, Fusco ML, Ilinykh PA, Huang K, Wirchnianski AS, James RM, Herbert AS, Hui S, Goodwin E, Howell KA, Kailasan S, Aman MJ, Walker LM, Dye JM, Bukreyev A, Chandran K, Saphire EO. 2019. Structural basis of broad ebolavirus neutralization by a human survivor antibody. Nat Struct Mol Biol 26:204–212. https://doi.org/10.1038/s41594-019-0191-4.
30. Wec AZ, Herbert AS, Murin CD, Nyakatura EK, Abelson DM, Fels JM, He S, James RM, de La Vega M-A, Zhu W, Bakken RR, Goodwin E, Turner HL, Jangra RK, Zeitlin L, Qiu X, Lai JR, Walker LM, Ward AB, Dye JM, Chandran K, Bornholdt ZA. 2017. Antibodies from a human survivor define sites of vulnerability for broad protection against Ebolaviruses. Cell 169:878–890.e15. https://doi.org/10.1016/j.cell.2017.04.037.
31. Bornholdt ZA, Turner HL, Murin CD, Li W, Sok D, Souders CA, Piper AE, Goff A, Shamblin JD, Wollen SE, Sprague TR, Fusco ML, Pommert KBJ, Cavacini LA, Smith HL, Klempner M, Reimann KA, Krauland E, Gerngross TU, Wittrup KD, Saphire EO, Burton DR, Glass PJ, Ward AB, Walker LM. 2016. Isolation of potent neutralizing antibodies from a survivor of the 2014 Ebola virus outbreak. Science 351:1078–1083. https://doi.org/10.1126/science.aad5788.
32. Lee JE, Fusco ML, Hessell AJ, Oswald WB, Burton DR, Saphire EO. 2008. Structure of the Ebola virus glycoprotein bound to an antibody from a human survivor. Nature 454:177–182. https://doi.org/10.1038/nature07082.
33. Gehring G, Rohrmann K, Atenchong N, Mittler E, Becker S, Dahlmann F, Pöhlmann S, Vondran FWR, David S, Manns MP, Ciesek S, von Hahn T. 2014. The clinically approved drugs amiodarone, dronedarone and verapamil inhibit filovirus cell entry. J Antimicrob Chemother 69:2123–2131. https://doi.org/10.1093/jac/dku091.
34. Johansen LM, DeWald LE, Shoemaker CJ, Hoffstrom BG, Lear-Rooney CM, Stossel A, Nelson E, Delos SE, Simmons JA, Grenier JM, Pierce LT, Pajouhesh H, Lehár J, Hensley LE, Glass PJ, White JM, Olinger GG. 2015. A screen of approved drugs and molecular probes identifies therapeutics with anti-Ebola virus activity. Sci Transl Med 7:290ra89. https://doi.org/10.1126/scitranslmed.aaa5597.
35. Ren J, Zhao Y, Fry EE, Stuart DI. 2018. Target identification and mode of action of four chemically divergent drugs against Ebolavirus infection. J Med Chem 61:724–733. https://doi.org/10.1021/acs.jmedchem.7b01249.
36. DeWald LE, Dyall J, Sword JM, Torzewski L, Zhou H, Postnikova E, Kollins E, Alexander I, Gross R, Cong Y, Gerhardt DM, Johnson RF, Olinger GG, Holbrook MR, Hensley LE, Jahrling PB. 2018. The calcium channel blocker bepridil demonstrates efficacy in the murine model of Marburg virus disease. J Infect Dis 218:S588–S591. https://doi.org/10.1093/infdis/jiy332.
37. Johansen LM, Brannan JM, Delos SE, Shoemaker CJ, Stossel A, Lear C, Hoffstrom BG, Dewald LE, Schornberg KL, Scully C, Lehár J, Hensley LE, White JM, Olinger GG. 2013. FDA-approved selective estrogen receptor modulators inhibit Ebola virus infection. Sci Transl Med 5:190ra79. https://doi.org/10.1126/scitranslmed.3005471.
38. Zhao Y, Ren J, Harlos K, Jones DM, Zeltina A, Bowden TA, Padilla-Parra S, Fry EE, Stuart DI. 2016. Toremifene interacts with and destabilizes the Ebola virus glycoprotein. Nature 535:169–172. https://doi.org/10.1038/nature18615.
39. Bortz RH, Wong AC, Grodus MG, Recht HS, Pulanco MC, Lasso G, Anthony SJ, Mittler E, Jangra RK, Chandran K. 2020. A virion-based assay for glycoprotein thermostability reveals key determinants of filovirus entry and its inhibition. J Virol 94:e00336-20. https://doi.org/10.1128/JVI.00336-20.
40. Lu F, Liang Q, Abi-Mosleh L, Das A, De Brabander JK, Goldstein JL, Brown MS. 2015. Identification of NPC1 as the target of U18666A, an inhibitor of lysosomal cholesterol export and Ebola infection. Elife 4:e12177. https://doi.org/10.7554/eLife.12177.
41. Cheshenko N, Pierce C, Herold BC. 2018. Herpes simplex viruses activate phospholipid scramblase to redistribute phosphatidylserines and Akt to the outer leaflet of the plasma membrane and promote viral entry. PLoS Pathog 14:e1006766. https://doi.org/10.1371/journal.ppat.1006766.
42. Jambunathan N, Charles A-S, Subramanian R, Saied AA, Naderi M, Rider P, Brylinski M, Chouljenko VN, Kousoulas KG. 2015. Deletion of a predicted β-sheet domain within the amino terminus of herpes simplex virus glycoprotein K conserved among alphaherpesviruses prevents virus entry into neuronal axons. J Virol 90:2230–2239. https://doi.org/10.1128/JVI.02468-15.
43. Zhang P, Monteiro da Silva G, Deatherage C, Burd C, DiMaio D. 2018. Cell-penetrating peptide mediates intracellular membrane passage of human papillomavirus L2 protein to trigger retrograde trafficking. Cell 174:1465–1476.e13. https://doi.org/10.1016/j.cell.2018.07.031.
44. Assetta B, Morris-Love J, Gee GV, Atkinson AL, O'Hara BA, Maginnis MS, Haley SA, Atwood WJ. 2019. Genetic and functional dissection of the role of individual 5-HT2 receptors as entry receptors for JC polyomavirus. Cell Rep 27:1960–1966.e6. https://doi.org/10.1016/j.celrep.2019.04.067.
45. Takada A, Robison C, Goto H, Sanchez A, Murti KG, Whitt MA, Kawaoka Y. 1997. A system for functional analysis of Ebola virus glycoprotein. Proc Natl Acad Sci U S A 94:14764–14769. https://doi.org/10.1073/pnas.94.26.14764.
46. Whelan SP, Ball LA, Barr JN, Wertz GT. 1995. Efficient recovery of infectious vesicular stomatitis virus entirely from cDNA clones. Proc Natl Acad Sci U S A 92:8388–8392. https://doi.org/10.1073/pnas.92.18.8388.
47. Jeffers SA, Sanders DA, Sanchez A. 2002. Covalent modifications of the Ebola virus glycoprotein. J Virol 76:12463–12472. https://doi.org/10.1128/jvi.76.24.12463-12472.2002.
48. Kleinfelter LM, Jangra RK, Jae LT, Herbert AS, Mittler E, Stiles KM, Wirchnianski AS, Kielian M, Brummelkamp TR, Dye JM, Chandran K. 2015. Haploid genetic screen reveals a profound and direct dependence on

cholesterol for hantavirus membrane fusion. mBio 6:e00801. https://doi.org/10.1128/mBio.00801-15.

49. Smith SM, Kane SE, Gal S, Mason RW, Gottesman MM. 1989. Glycosylation of procathepsin L does not account for species molecular-mass differences and is not required for proteolytic activity. Biochem J 262:931–938. https://doi.org/10.1042/bj2620931.
50. Kane SE. 1993. Mouse procathepsin L lacking a functional glycosylation site is properly folded, stable, and secreted by NIH 3T3 cells. J Biol Chem 268:11456–11462.
51. WHO. 2020. 10th Ebola outbreak in the Democratic Republic of the Congo declared over; vigilance against flare-ups and support for survivors must continue. WHO, Geneva, Switzerland. https://www.who.int/news/item/25-06-2020-10th-ebola-outbreak-in-the-democratic-republic-of-the-congo-declared-over-vigilance-against-flare-ups-and-support-for-survivors-must-continue.